Practical Capacity Fading Model for Li-Ion Battery Cells in Electric Vehicles

Long Lam and Pavol Bauer, *Senior Member, IEEE*

***Abstract*—This paper proposes a practical capacity fading model for Li-ion cells based on real operating conditions in electric vehicles (EVs). Numerous $LiFePO_4$ cells have been cycled with a current profile containing regenerative braking to determine the capacity fading rate. The cells have been cycled at different temperatures with different initial state of charges, depth of discharges, or C-rates. From the experiments, an empirical model is constructed, which is capable of modeling the capacity fading in EV battery cells under most operating conditions. The capacity fading model can be used to estimate the state of health of EV battery cells, and simple ways to optimize the battery lifetime are proposed.**

***Index Terms*—Capacity fading model, electric vehicle (EV) battery, $LiFePO_4$, regenerative braking.**

I. Introduction

THE REST value of electric vehicles (EVs) is greatly determined by the state of health (SoH) of the Li-ion EV battery. With more insight in the SoH development of EV batteries, electric driving will become cheaper. In Li-ion cells, many degradation mechanisms occur and are accelerated by various internal and external stress factors [1]. The degradation mechanisms cause the battery cell performance to deteriorate, which is used to determine the SoH of the cell. However, the SoH is a subjective term and which performance characteristics to choose as SoH indicators depend on the specifications of the application. When the SoH becomes 0%, the end–of-life (EoL) condition has been fulfilled. By convention, for EV batteries, the EoL condition is reached when the battery capacity has dropped to 80% of the nominal capacity at reference conditions. Hence, the permanent capacity loss, i.e., capacity fading, is chosen as the SoH indicator for EV applications.

Capacity fading does not only occur from usage, but also under storage. These are, respectively, named cycling and calendar losses. Furthermore, capacity fading can be divided into true capacity fading and rate capability loss [2]. True capacity fading is capacity fading as a result of lithium ion and active material loss, and is determined independent from the current. On the other hand, rate capability loss is capacity fading due to the cell impedance growth and depends on the current level; the cell impedance growth causes the minimum cutoff voltage to be reached at a higher state of charge (SoC) than compared to a new cell. In the literature, the distinction between true capacity fading and rate capability loss is often not made and the capacity fading determined with 1 C is used.

Numerous experiments have been conducted in the literature to determine the capacity fading rate for Li-ion cells and the associated stress factors accelerating capacity fading. However, different Li-ion types have been tested under different conditions in the experiments, which have led to dissimilar results. In the literature, the capacity fading rate was modeled with either a radical and linear function [3], [4], a quadratic and linear function [2], or simply a linear function [5], [6]. Some authors found that a larger depth of discharge (DoD) accelerates capacity fading [4], [7], which corresponds to the well-known logarithmic curve of cycle life as a function of DoD [8]. Other authors observed that the DoD does not accelerate capacity fading [9], [10]. A high initial SoC resulted in a higher capacity fading rate for cycling [7], but was found to show contradicting results for cells under storage. For calendar losses, a high SoC was found to either have a significant influence on the capacity fading [11] or having no influence at all [12]. In regard to temperature, no conflicting results have been found. Experimental results have shown that high temperature is a stress factor and can be modeled with the Arrhenius equation [3], [5], [13]. Furthermore, overdischarge [14], overcharge, and high C-rates [10] were also observed to enhance the capacity fading rate.

The experiments in the literature were primarily conducted with $LiCoO_2$, NCA, and more recently $LiFePO_4$ cells. The different capacity fading rates and DoD influences are mainly caused by the use of different Li-ion types. The DoD is defined as the SoC discharged from 100% SoC [15] and experiments in the literature measuring the DoD influence always start at 100% SoC. In EVs, however, the SoC will be rarely 100% and a driving cycle will start at various SoCs. Furthermore, most experiments are conducted with a constant current discharge, while EVs experience a dynamic profile with regenerative braking. The experiments that do include regenerative braking in the cycling profile use a dynamic profile with varying C-rate levels [9], [16]. The C-rate level is assumed to have no direct effect on the capacity fading, only indirectly in the form of temperature rise due to ohmic heating [17], [18].

In this paper, the capacity fading rate of $LiFePO_4$ cells will be characterized and the influences of various stress factors on

Manuscript received June 5, 2012; revised August 31, 2012; accepted December 9, 2012. Date of current version June 6, 2013. This work was supported by High Tech Automotive Systems (HTAS) under project Databox project code HSH10001 and project Commercial Drivetrain Technology project code HTASE10205. Recommended for publication by Associate Editor J. Cao.

L. Lam was with the Department of Electrical Sustainable Energy, Delft University of Technology, 2628 CD Delft, The Netherlands. He is now with Ecofys, 3526 KL Utrecht, The Netherlands (e-mail: L.Lam@ecofys.com).

P. Bauer is with the Department of Electrical Sustainable Energy, Delft University of Technology, 2628 CD Delft, The Netherlands (e-mail: P.Bauer@TUDelft.nl).

Color versions of one or more of the figures in this paper are available online at http://ieeexplore.ieee.org.

Digital Object Identifier 10.1109/TPEL.2012.2235083

the capacity fading will be modeled based on practical operating conditions in EVs. Only the true capacity fading has been determined, because that is the permanent capacity lost in the cell. Capacity fading due to rate capability loss can be regained with a smaller current. Rate capability losses can be determined numerically if the cell impedance growth is known. Additionally, only cycling losses have been characterized and calendar losses have been neglected. Calendar losses in Li-ion cells are very small with a few percentages per year at room temperature [12] and will, therefore, have a negligible effect on the capacity fading compared to cycling losses.

Numerous cells are cycled with a current profile containing regenerative braking, but with a fixed discharge and recharge C-rate. The capacity fading will be a function of the charge processed by the cell instead of cycle number for various reasons. A cycle is not clearly defined for a current profile with regenerative braking. In an EV, the battery is not always charged to the same SoC, so the conventional definition of a cycle cannot be used. More importantly, the capacity fading of cells discharged with different DoDs as a function of cycles will lead to a wrong comparison, as the charge processed in each cell is different. The charge processed in the cell is the time integral of the current through the cell. Furthermore, the incremental DoD (ΔDoD) will be used instead of the DoD. The DoD is a measure from 100% SoC, whereas the ΔDoD is the difference in SoC from the initial and final SoCs before a cell is recharged to the initial SoC. Experiments with different initial SoCs, ΔDoDs, temperatures, discharge C-rates, and regenerative braking C-rates with values based on practical operating conditions in EVs are conducted. Overcharge and overdischarge are not characterized, since it is assumed that the battery management system (BMS) will keep the cell voltage within the specified limits. Finally, a practical capacity fading model with empirical equations is obtained.

This paper is organized as follows. In Section II, the experimental test procedure is explained. Section III describes the measurement results of the stress factors on the capacity fading rate and proposes empirical equations to model the stress factors. The empirical equations are combined in Section IV and simple ways to optimize the battery lifetime are suggested. Section V concludes this paper.

II. Experimental Test Procedure

A123 Systems' APR18650m1 $LiFePO_4$ cells with a nominal capacity of 1.1 Ah obtained from a third party vendor has been used in the experiment with a Maccor Series 2000 Automated Battery tester. The Maccor Series 2000 automated battery tester has 16 independent channels with a maximum rating of 10 V and 2 A. The battery tester logs the data on its own internal memory and writes it once a while to the PC. The cells were placed in a closed temperature-regulated chamber and initially change of the surface temperature of each cell has been monitored. The temperature change was, however, very small during a charge or discharge cycle, and the cell temperature was assumed to be equal to the temperature of the chamber.

Each cell has been cycled continuously with the current profile shown in Fig. 1 for ten weeks. A positive C-rate is discharge, a negative charging. The value and duration of the discharge and recharge C-rate periods in Fig. 1 are the mean discharge and regenerative braking C-rate level and duration determined from a real driving profile. In the different experiments, only the C-rate levels have been changed, and the duration of the discharge and recharge periods remained constant. After the cells have been discharged with the desired ΔDoD, the cells were recharged to the desired SoC with the recommended current 1.5 A [19]. The SoC used in the model is thermodynamic-SoC related to the open-circuit voltage instead of the engineering-SoC, which is the apparent SoC to the user [20]. The cells were rested after every 50% SoC processed. This way, cells discharged with different ΔDoDs were experienced an equal resting period. Each resting period in the experiment was 15 min long, which was chosen as a tradeoff between the general resting period of 1 h [21] and a minimum testing time. The voltage difference between 15 min rest and 1 h rest is approximately 3 mV for 1 C at 25 °C, which is acceptably small. After every 25 equivalent full cycles, the cell capacity was measured with a test cycle. Each cell was charged with the constant current constant voltage (CCCV) method. The cells were charged with 1.5 A up to 3.6 V and then charged at constant voltage until the current was lower than 0.01 C. To approximate the true capacity fading of the cells, each cell was not only charged with the CCCV method, but also discharged in the same way. The minimum cell voltage was set to 2.5 V to prevent overdischarge. Before each discharge and charge period in the capacity measurement test cycle, the cells were rested. After each test cycle, the cells were discharged to the desired SoC with a constant current and rested before cycled again.

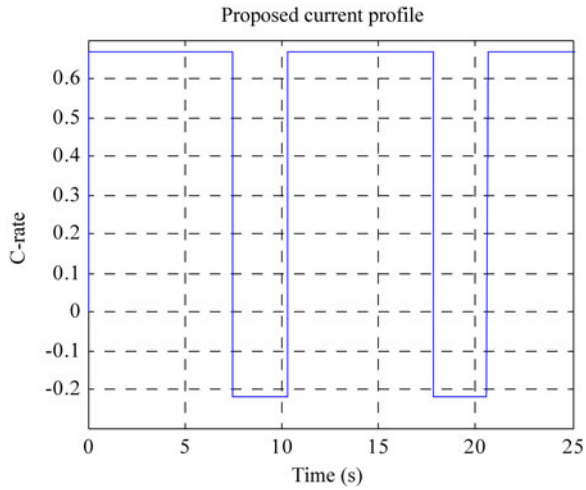

Fig. 1. Proposed current profile used in the cycling tests.

III. Modeling Stress Factors

To be able to distinguish the influence of the different stress factors on the capacity fading rate, the capacity fading rate of each cell was compared to the reference conditions. The reference conditions were chosen to be 90% initial SoC, 25% ΔDoD, and 25 °C, with discharging and regenerative braking C-rates of, respectively, 0.67 C and 0.22 C, as shown in Fig. 1.

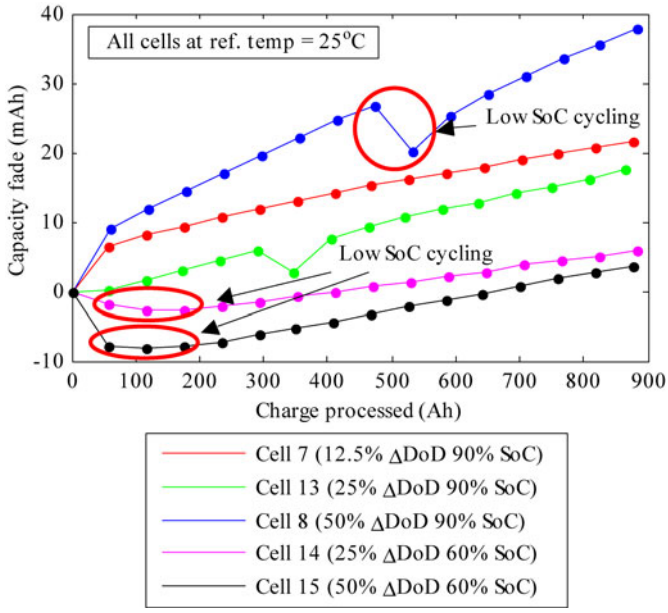

Fig. 2. Capacity fade determined for cells cycled at different SoC and ΔDoD versus the charge processed.

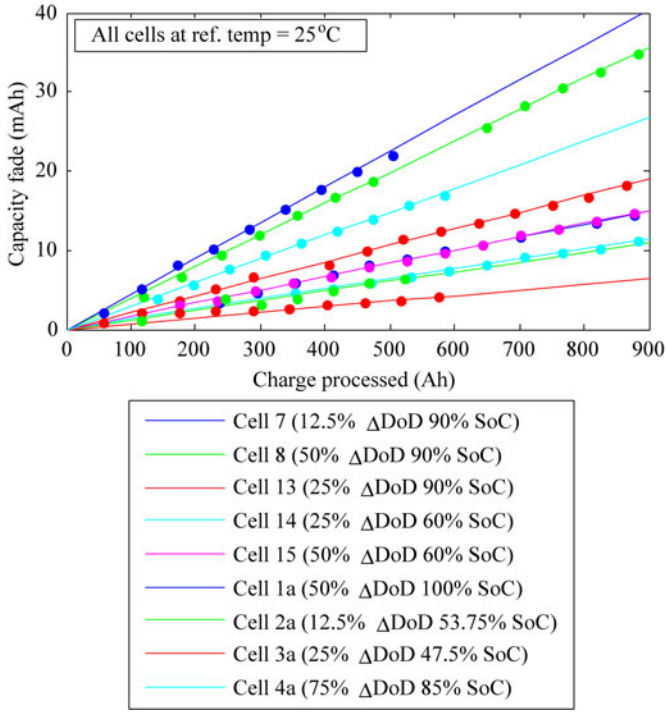

Fig. 3. Linear fit of the capacity fade for cells cycled at different SoCs and ΔDoDs versus the charge processed.

Only one or two test conditions have been varied in the life cycle experiments to test the influence of various stress factors.

In this section, first the stress factors SoC and ΔDoD are modeled with empirical equations. Then, the influence of the discharge C-rate is discussed. Next, the temperature stress factor is modeled. The influence of regenerative braking and the recharge C-rate is also investigated. Finally, this section is concluded by combining the stress factor models into a practical capacity fading model.

A. SoC and ΔDoD

The influence of the initial SoC and ΔDoD on the capacity fading rate has been determined by cycling cells with the proposed current profile at reference temperature. The capacity fade as a function of the amount of charge processed in the cell is shown in Fig. 2. The capacity fading rate is linear and slightly saturates. The capacity fading rate can, therefore, be accurately modeled by a combined linear and radical function. Between the first and second data point, the capacity fading does not follow the general trend. This is the kick-in period, during which the cell still has to be stabilized. The cells that reach a low SoC, indicated with *low SoC cycling* in Fig. 2, even experience capacity rise. This may be caused by a structural change in the cell at low SoCs. *Cell 8* experienced low SoC cycling as a result of a programming error, which also led to an increase in cell capacity. The capacity fading rate is eventually restored at a lower amount of total capacity fade. This leads to the conclusion that low SoC cycling indeed causes a structural capacity gain for cells that have not experienced low SoC cycling before, but does not have an influence on the capacity fading rate.

However, the goal of this section is to model the general capacity fading trend under influence of different SoCs and ΔDoDs. Therefore, the kick-in period of the cell and capacity gain due to low SoC cycling will not be characterized. The capacity fading rate can be approximated by a linear function. By neglecting the kick-in period and other anomalies, the capacity fading rates shown in Fig. 3 are obtained. The linear fit has been obtained through curve fitting in MATLAB and the adjusted R2 of each fit is at least 0.90, with an adjusted R^2 of 0.99 for most fits. Additional cells have been cycled with different initial SoCs and ΔDoDs for six weeks, and the measurement results are also shown in Fig. 3 with the suffix "a."

The capacity fade shown in Fig. 3 is the relative capacity fade to illustrate the capacity fading rate and not the actual capacity fade occurred in the cell at a certain amount of charge processed. Fig. 3 shows that high initial SoCs and large ΔDoDs result in a high capacity fading rate. However, the initial SoC of *Cell 4a* is nearly as high as *Cell 8* and the ΔDoD is much larger, while the capacity fading rate is much lower. This seems counterintuitive, as the larger ΔDoDs should cause more capacity fading. A comparison between Cell 3a and Cell 2a shows similar results. This can be explained by not using the initial SoC and ΔDoD to characterize the capacity fading rate, but using the average SoC and the deviation from the average SoC, as proposed in [17]. Since calendar fading is neglected in the model, the SoC will be a function of the charge processed instead of time. The average SoC, $\mathrm{SoC}_{\mathrm{avg}}$, in a predefined period is determined by

$$\mathrm{SoC}_{\mathrm{avg}} = \frac{1}{\Delta \mathrm{Ah}_m} \int_{\mathrm{Ah}_{m-1}}^{\mathrm{Ah}_m} \mathrm{SoC}\,(\mathrm{Ah})\, d\mathrm{Ah} \tag{1}$$

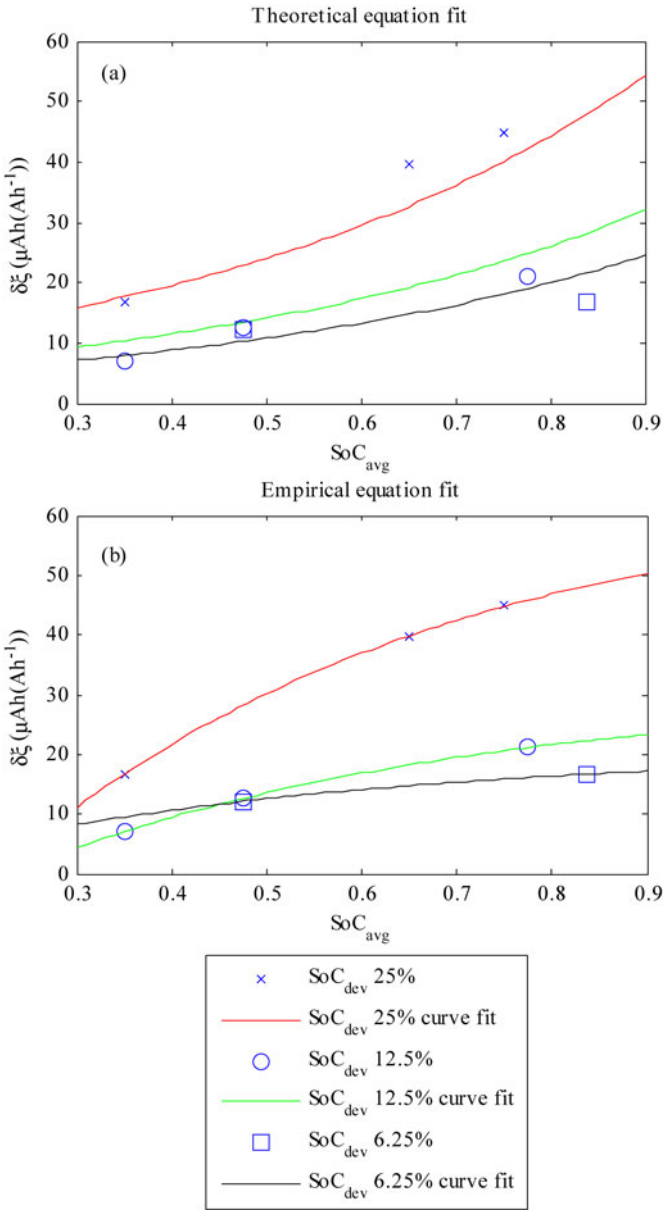

Fig. 4. Capacity fading rate versus $\mathrm{SoC_{avg}}$ for different $\mathrm{SoC_{dev}}$ and the curve fits with the (a) theoretical equation and (b) empirical equation.

where Ah_{m-1} is the initial amount of charge processed before the $\mathrm{SoC_{avg}}$ determination, Ah_m is the final amount in the predefined period, and $\Delta\mathrm{Ah}_m$ is $\mathrm{Ah}_m - \mathrm{Ah}_{m-1}$. Using $\mathrm{SoC_{avg}}$, the SoC deviation $\mathrm{SoC_{dev}}$ is then calculated with

$$\mathrm{SoC_{dev}} = \sqrt{\frac{3}{\Delta\mathrm{Ah}_m}\int_{\mathrm{Ah}_{m-1}}^{\mathrm{Ah}_m}\left(\mathrm{SoC}\,(\mathrm{Ah}) - \mathrm{SoC_{avg}}\right)^2 d\mathrm{Ah}}. \quad (2)$$

$\mathrm{SoC_{dev}}$ is the normalized standard deviation from $\mathrm{SoC_{avg}}$; a cell with an initial SoC of 100% cycled with 100% ΔDoD corresponds to 50% $\mathrm{SoC_{dev}}$ with a $\mathrm{SoC_{avg}}$ of 50%. The capacity fading rate of various cells is plotted in Fig. 4 as a function of $\mathrm{SoC_{avg}}$. The operating conditions initial SoC and ΔDoD have been transformed into $\mathrm{SoC_{avg}}$ and $\mathrm{SoC_{dev}}$.

TABLE I
CAPACITY FADING MODEL PARAMETERS

k_{s1}	-4.092E-4	k_{s3}	1.408E-5
k_{s2}	-2.167	k_{s4}	6.130

In [17], theoretical equations were proposed to describe the influence of $\mathrm{SoC_{avg}}$ and $\mathrm{SoC_{dev}}$ on the capacity fading rate based on crack propagation. The capacity fading rate was exponentially dependent on both $\mathrm{SoC_{avg}}$ and $\mathrm{SoC_{dev}}$. Furthermore, the proposed capacity fading equation was linearly dependent on the charge processed, corresponding to the measurements in Fig. 3. Using the Surface Fitting Tool in MATLAB, the curve fits of the theoretical equations were obtained with an adjusted R2 of 0.86. The curve fits are shown in Fig. 4(a). The theoretical equations are able to capture the expected influence of $\mathrm{SoC_{avg}}$ and $\mathrm{SoC_{dev}}$; the higher the $\mathrm{SoC_{avg}}$ or $\mathrm{SoC_{dev}}$, the higher the capacity fading rate. However, the capacity fading rate modeled by the theoretical equations deviate up to 30% from the measurements, limiting the accuracy of the model. Therefore, an empirical equation is proposed, which can model the measured capacity fading rates more accurately

$$\delta\xi(\mathrm{SoC_{avg}}, \mathrm{SoC_{dev}}) = k_{s1}\mathrm{SoC_{dev}} \cdot e^{(k_{s2}\cdot\mathrm{SoC_{avg}})} + k_{s3}e^{(k_{s4}\cdot\mathrm{SoC_{dev}})}. \quad (3)$$

The unit of the capacity fading rate $\delta\xi$ is Ah faded per Ah processed. Following [17], the capacity fading rate was initially modeled as a multiplication of the $\mathrm{SoC_{avg}}$ and $\mathrm{SoC_{dev}}$ exponential equations, but the measurement results could not be modeled accurately enough. Consequently, first an empirical equation for the capacity fading rate was obtained by setting the parameter with the least variations, $\mathrm{SoC_{dev}}$, as a constant and curve fitting the measurements with a standard exponential function and $\mathrm{SoC_{avg}}$ as a variable in the MATLAB Curve Fitting Tool. Then, after analyzing the $\mathrm{SoC_{dev}}$ influence on the measured capacity fading rates, (3) and parameters k_{s1} to k_{s4} were obtained through curve fitting in the MATLAB Surface Fitting Tool with both $\mathrm{SoC_{avg}}$ and $\mathrm{SoC_{dev}}$ as variables. The parameters k_{s1} to k_{s4} are given in Table I. The curve fits of (3) for different $\mathrm{SoC_{dev}}$ are shown in Fig. 4(b); the adjusted R2 of the fit is 0.99.

In the curve fit, the 12.5% $\mathrm{SoC_{dev}}$ and 6.25% $\mathrm{SoC_{dev}}$ curves cross one another. This suggests that from a certain $\mathrm{SoC_{avg}}$ and lower, the cells will have a longer cycle life if a larger $\mathrm{SoC_{dev}}$ is experienced, which does not seem intuitive at all. Furthermore, the curve fits may result in a negative capacity fading rate at low $\mathrm{SoC_{avg}}$. These irregularities are caused by the fact that (3) was obtained from a limited amount of data points. The capacity fading rate at low $\mathrm{SoC_{avg}}$ has not been investigated for certain $\mathrm{SoC_{dev}}$ values, resulting in inconclusive capacity fading rates for low $\mathrm{SoC_{avg}}$. Nevertheless, (3) is sufficient to capture the influence of the $\mathrm{SoC_{avg}}$ and $\mathrm{SoC_{dev}}$ on the capacity fading behavior of the cell in most of the SoC region, if $\Delta\mathrm{Ah}_m$ in (1) and (2) is taken over a complete driving cycle. A complete driving cycle would consist of a period of driving, followed by a period of charging until the EV is driven again. From the capacity

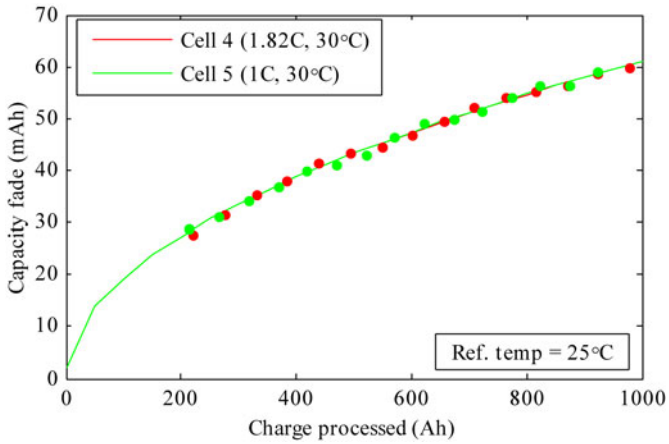

Fig. 5. Capacity fade of two cells cycled with different discharge C-rates versus the charge processed.

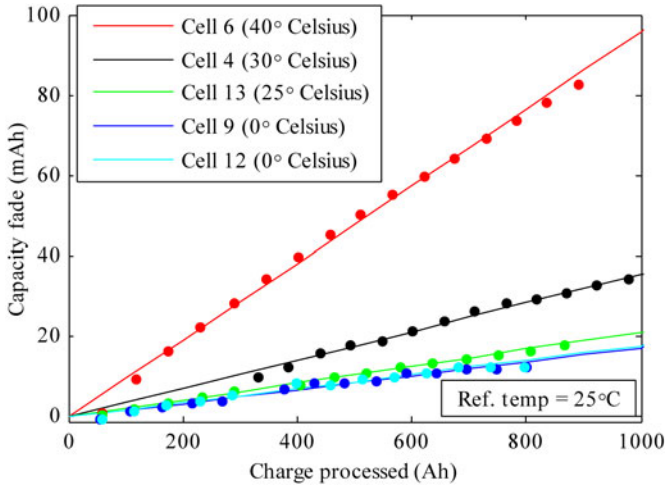

Fig. 6. Linear fit of the capacity fade of cells cycled at different temperatures versus the charge processed.

fading analysis of cells discharged from different initial SoCs and ΔDoDs, it can be concluded that a lower average SoC and/or a lower ΔDoD results in a lower capacity fading rate. However, whether the theoretical model proposed by Millner [17] or the proposed empirical model is more accurate to model the actual influence of $\mathrm{SoC_{avg}}$ and $\mathrm{SoC_{dev}}$ cannot be concluded due to insufficient data points. More cells need to be cycled at different $\mathrm{SoC_{avg}}$ and $\mathrm{SoC_{dev}}$ to be able to draw solid conclusions on which set of equations models the capacity fading in EV Li-ion cells more accurately.

B. Discharge C-Rate

In the literature, no definitive reports have been found on whether high discharge C-rates directly cause accelerated capacity fading, or if it is a result of ohmic heating. This has been investigated by cycling two cells with the proposed current profile under the same conditions at 30 °C, where only the discharge C-rate has been varied. Since the temperature chamber keeps the cell at a constant temperature, cell temperature change due to ohmic heating will be small. The capacity fade of the cells has been curve fitted with a combination of a linear and radical function to obtain the capacity fading rate accurately, which is depicted in Fig. 5. The capacity fade shown in Fig. 5 is the capacity fade obtained with the curve fit, and not the actual capacity fade in the cells.

As can be seen from Fig. 5, the capacity fading rate of both cells is overlapping. It can, therefore, be concluded that different discharge C-rates around room temperature do not contribute to additional capacity fade, under the condition that the C-rates do not exceed the maximum rating of the cell. The discharge C-rate is far under the maximum rated C-rate, and it is possible that high C-rates near the maximum will introduce additional capacity fade. Batteries in EVs, however, also operate with a C-rate far under the maximum specifications and are often oversized to have sufficient driving range. The discharge C-rate will, therefore, most likely not introduce additional capacity fade. This is under the assumption that the BMS will not let the battery overdischarge. Nonetheless, high C-rates cause ohmic heating, which results in cell temperature rise, and therefore still cause accelerated capacity fading indirectly.

C. Temperature

The influence of temperature on the capacity fading rates has been determined by cycling cells at different temperatures. Cells were cycled at −20 °C, 0 °C, 25 °C, and 40 °C. The cell cycled at −20 °C experienced such severe capacity fading that the capacity fading rate could not be characterized, and has been omitted from the temperature stress factor analysis. The linear fit of the capacity fading rates for the other cells is given in Fig. 6. In the previous section, it was also concluded that the discharge C-rate did not have a direct influence on the capacity fading rate, so the cell cycled at 30 °C can also be included in the temperature analysis, as shown in Fig. 6. The erroneous initial capacity fade measurements of the 30 °C cell due to a programming error have been omitted.

In line with the general expectation, the cycle life of Li-ion cells severely reduces above room temperature. At the end of the experiment, the cells have been brought back to reference temperature to determine the true capacity fading. The measured capacity at 25 °C after the experiments was compared to the measurements conducted before the experiments and the capacity fading rate was corrected. The measured and corrected capacity fading rates are shown in Fig. 7. The capacity fading rate of *Cell 9* is much lower than *Cell 12*, even though both cells were cycled at 0 °C. This is explained by the fact that both cells were still in their kick-in period when the capacity at reference temperature was initially determined. In this kick-in period, the cell structure may not be stabilized yet, causing the measured capacity of each subsequent cycle to possibly deviate from the previous cycle. This resulted in an inaccurate measurement of the temperature-dependent capacity change. To accurately determine the amount of reversible capacity loss, every test cycle, the capacity at reference temperature should have been measured. Unfortunately, due to practical issues, this was not possible.

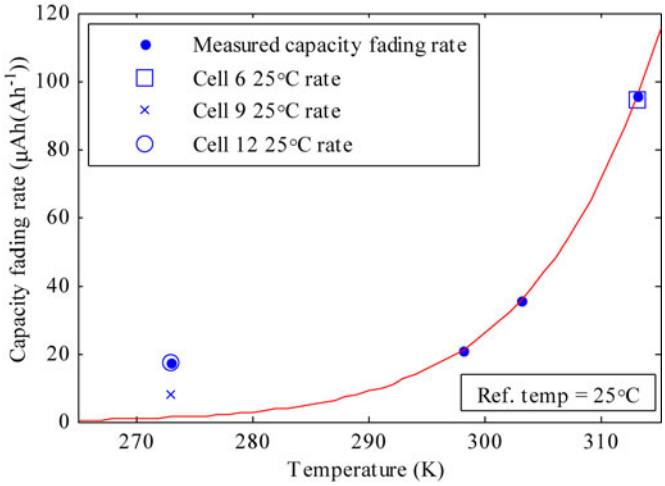

Fig. 7. Measured capacity fading rates versus temperature. The capacity fading rates corrected to 25 °C have been fitted with the Arrhenius equation. The capacity fading rate at 0 °C has been excluded from the fit.

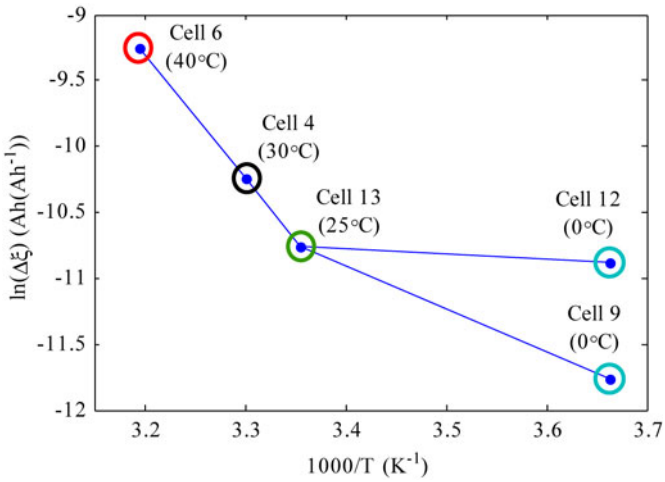

Fig. 8. Natural logarithm of the capacity fading rate at different temperatures corrected for 25 °C versus 1000/T.

The temperature dependence of the capacity fading rate has been analyzed with the Arrhenius equation

$$\delta\xi(T) = \delta\xi_{\text{ref}} \cdot e^{\left(-\frac{E_a}{R}\left(\frac{1}{T}-\frac{1}{T_{\text{ref}}}\right)\right)} \tag{4}$$

where $\delta\xi_{\text{ref}}$ is the capacity fading rate under the reference conditions (*Cell 13*), R is the gas constant, E_a is the activation energy, T is the temperature, and T_{ref} is the reference temperature, both in Kelvin. The natural logarithm of the capacity fading rates has been plotted against 1000/T in Fig. 8 to see whether the capacity fading rates follow the Arrhenius equation.

From Fig. 8, it can be seen that the capacity fading rate for temperatures above 25 °C is linear with 1000/T, while the capacity fading rate at 0 °C does not fit the linear trend. This means that the Arrhenius equation is at least valid for temperatures above 25 °C, and at lower temperatures, another capacity fading mechanism is present. In Fig. 7, the capacity fading rate at 0 °C is excluded from the fit with (4). $\delta\xi_{\text{ref}}$ is the capacity fading rate at reference temperature and E_a is 78.06 kmol/J.

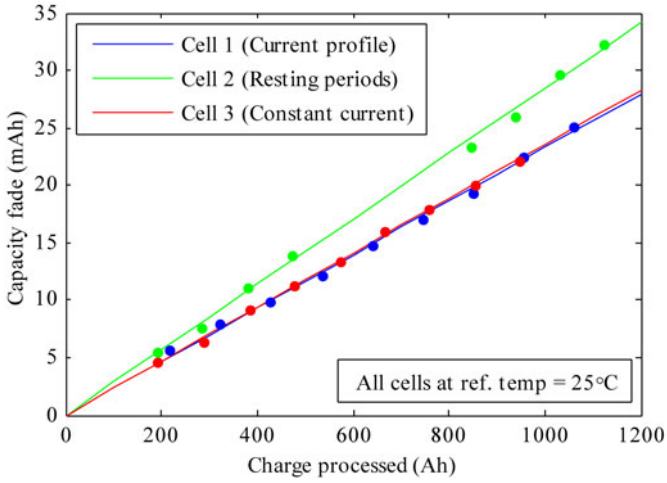

Fig. 9. Linear fit of cells cycled with different current profiles versus the charge processed.

It can be seen that capacity fading rate at 0 °C is higher than the rate predicted by the Arrhenius equation, caused by another capacity fading mechanism. This is most likely lithium plating due to the recharge of regenerative braking and normal charging. Therefore, the capacity fading rate modeled by (4) is valid for temperatures above 25 °C, insufficient below 0 °C, and possibly too optimistic between 0 °C and 25 °C. This should be confirmed with additional capacity fading measurements at various temperatures, since the amount of data points from the conducted measurements is limited.

D. Regenerative Braking C-Rate

To investigate the influence of regenerative braking on the capacity fading, the capacity fading of a cell cycled with the proposed current profile is compared to a cell cycled with a constant discharge current and a cell cycled with resting periods instead of regenerative braking periods. The other operating conditions were equal for all three cells and the cells have been cycled at 25 °C. The linear fit of the capacity fading rates is shown in Fig. 9. The cells discharged with regenerative braking and constant current show the same capacity fading rate. This means that the capacity fading rate is not influenced by regenerative braking with typical EV C-rates at reference temperature.

However, the cell with resting periods instead of recharging periods (*Cell 2*) shows a higher capacity fading rate than the other two cells. Possible reasons are that the short resting periods have a negative influence on the capacity of the cell or that the quality of the tested cell was worse than the other cells. Furthermore, the testing equipment skipped three test cycles during the experiment, as seen in Fig. 9. The results of Cell 2 are, therefore, deemed to be inconclusive. To test whether resting periods have an influence on the capacity fading rate of the cell, future research may include the cycling of cells with resting periods of different lengths.

In the analysis of the temperature stress factor, it was determined that at 0 °C, regenerative braking might have had an influence on the capacity fading as a result of lithium plating. This was investigated by cycling a cell with a higher

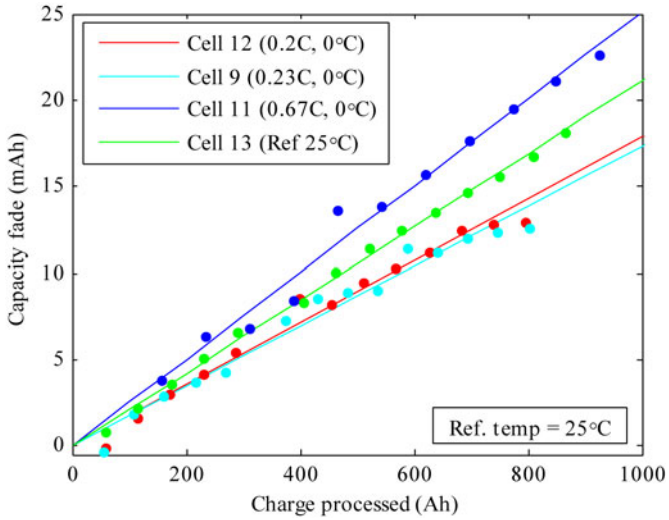

Fig. 10. Linear fit of cells cycled at 0 °C with different regenerative braking C-rates and the cell cycled at reference conditions.

regenerative braking C-rate in the proposed current profile. A comparison between the linear fit of the capacity fading rate of cells cycled at 0 °C with two different regenerative braking C-rates is shown in Fig. 10. The influence of an increased recharge C-rate is clearly visible. The cell with a higher regenerative braking C-rate clearly shows a higher capacity fading rate. It may be argued that even though the cells are constantly cooled, higher C-rates can still cause a temperature rise in the cell, which result in a higher capacity fading rate. However, the capacity fading of a cell cycled under the reference conditions is also shown in Fig. 10 and has a lower capacity fading rate than *Cell 11*. Even if the temperature rises in *Cell 11* as a result of a higher regenerative braking C-rate, it cannot explain the high capacity fading rate. It can, therefore, be concluded that the regenerative braking C-rate does have an influence on the capacity fading rate, which is mostly likely caused by lithium plating. In that case, lower temperatures and higher regenerative braking C-rates are expected to cause more capacity fade. However, not enough measurements have been conducted to confirm or quantify this effect.

IV. Capacity Fading Model

An empirical model describing the capacity fading in a $LiFePO_4$ cell is obtained by combining (3) and (4). The total capacity fade is a summation of the capacity fade occurred under the experienced operating conditions and is calculated by

$$\begin{aligned}&\xi(T, \mathrm{SoC_{avg}}, \mathrm{SoC_{dev}}, \mathrm{Ah}) \\ &= \sum_{i}^{E} \left(\left(k_{s1} \mathrm{SoC}_{\mathrm{dev},i} \cdot e^{(k_{s2} \cdot \mathrm{SoC}_{\mathrm{avg},i})} \right.\right. \\ &\quad \left.\left. + \; k_{s3} e^{k_{s4} \mathrm{SoC}_{\mathrm{dev},i}} \right) e^{\left(-\frac{E_a}{R} \left(\frac{1}{T_i} - \frac{1}{T_{\mathrm{ref}}} \right) \right)} \right) \mathrm{Ah}_i. \end{aligned} \quad (5)$$

Here, ξ is the total capacity fade, i is an event, which is an arbitrary determined period in which the stress factors are assumed to be constant, Ah_i is the charge processed during the event i, and E is the total number of events. The capacity fading model assumes that the temperature and SoC stress factors are not correlated, which has to be confirmed by additional cycling experiments. Furthermore, the capacity fading model is not valid for temperatures below 0 °C, because accelerated capacity fading was found to occur at low temperatures due to the C-rate of regenerative braking and charging. This effect is dependent on the recharge C-rate and temperature; the lower the temperature, the more severe the capacity fading is due the charging C-rate. Furthermore, between 0 °C and 25 °C, the model might be too optimistic, especially close to 0 °C. Above 25 °C, the regenerative braking C-rate was found to have no influence on capacity fading for typical EV C-rates. This means that between 0 °C and 25 °C, an optimum temperature exists for minimum capacity fading. Above this temperature, the capacity fading model corresponds to the measurements and the temperature stress factor is modeled with the Arrhenius equation; below this temperature, higher recharge C-rates will introduce additional capacity fading and the model is somewhat optimistic. Future work can include improving the proposed model with more measurements on the capacity fading rate under various conditions, modeling the charging C-rate effect at low temperatures and determining the optimum operating temperature.

To estimate the SoH, two types of SoH models exist: a weighted-throughput model and performance-based model [18]. A weighted-throughput model uses the possible throughput, e.g., charge processed, as SoH indicator. A performance-based model uses a measured parameter, e.g., capacity faded, to estimate the SoH. Since the capacity fading rate is linear in the empirical model, a weighted-throughput SoH model and a performance-based SoH model will yield the same results. The SoH of the cell can then be estimated with

$$\mathrm{SoH} = \left(1 - \frac{\xi}{0.2 Q_{\mathrm{nom}}} \right) \cdot 100\% \quad (6)$$

where Q_{nom} is the nominal capacity of the cell. It has to be noted that the SoH determined with (6) is based on the true capacity fading. The rate capability losses are not taken into account. However, generally the capacity measured with a current of 1 C is used to determine the capacity fading, which includes the rate capability losses. To determine the rate capability losses, the internal cell impedance growth has to be modeled. By incorporating the capacity fading model into a circuit-based model with impedance growth, the cell voltage can be accurately modeled under various operating conditions [22], [23], [24]. The rate capability losses are numerically determined by investigating at which SoC the minimum cutoff voltage is reached. The rate capability losses can then be added to (5) to determine the 1 C SoH of the cell.

From the capacity fading measurement results, several simple suggestions for battery lifetime optimization can be made. For an optimal battery lifetime, the $\mathrm{SoC_{avg}}$ and $\mathrm{SoC_{dev}}$ should be as low as possible, without the risk of overdischarge. This means that the battery should only be charged with enough energy for the upcoming trip, with an additional charge of approximately 10% SoC to prevent overdischarge. This can be achieved through

improved SoC controllers [25], [26], charge equalizers [27], [28], smarter chargers [29], or a hybrid battery/fuel [30] or battery/capacitor storage system [31], [32], [33]. Furthermore, regenerative braking should not be employed until the battery has been heated to the optimal operating temperature. Finally, proper thermal management will also extent the battery lifetime.

The capacity fading for other types than $LiFePO_4$ will most likely be different except the high-temperature influence, as the capacity fading is strongly dependent on cathode and anode material. For certain types of anodes, at low temperatures, the recharge C-rate will not accelerate capacity fading. Also, the influence of the average SoC and SoC deviation will be different for different Li-ion types; some types may even show accelerated capacity fading if the average SoC is too low or the SoC deviation influence is much stronger than the average SoC. Therefore, only for $LiFePO_4$ cells, it is confirmed that cycling with a low average SoC results in low capacity fading. With experiments similar to the ones in this paper, the effect of the average SoC and SoC deviation can be determined for other Li-ion cell types.

V. Conclusion

An empirical capacity fading model for EV cells is presented in this paper. The model is obtained by cycling $LiFePO_4$ cells with a current profile including regenerative braking. The cells have been cycled at different temperatures, initial SoCs, ΔDoDs, discharge C-rates, and regenerative braking C-rates based on real operating conditions. From the experiments, it was concluded that the capacity fading is low for a low average SoC and a low SoC deviation from the average SoC during cycling. High discharge C-rates and regenerative braking did not directly introduce additional capacity fading for typical EV battery C-rates at room temperature. However, the temperature rise due to ohmic heating would accelerate capacity fading. The temperature influence on capacity fading has been modeled with the Arrhenius equation, but at 0 °C, another capacity fading mechanism was observed. At low temperatures, the capacity fading is accelerated by high recharging C-rates, which is more profound as the temperature drops. Unfortunately, not enough measurements have been conducted to quantify this effect. The proposed capacity fading model is, therefore, valid above 25 °C, insufficient below 0 °C, and possible too optimistic between 0 °C and 25 °C, especially near 0 °C. However, the proposed model is only based on a limited number of measured capacity fading rates, and more measurements should be conducted to confirm the accuracy of the model. Nonetheless, it can be concluded that the battery lifetime can be optimized by keeping the SoC low and only charging enough energy for the upcoming trip, preventing regenerative braking at low temperatures and proper thermal management.

References

[1] J. Vetter, P. Novák, M. R. Wagner, C. Veit, K. C. Möller, J. O. Besenhard, M. Winter, M. Wohlfahrt-Mehrens, C. Vogler, and A. Hammouche, "Ageing mechanisms in lithium-ion batteries," *J. Power Sources*, vol. 147, no. 1/2, pp. 269–281, 2005.

[2] P. Ramadass, B. Haran, R. White, and B. N. Popov, "Mathematical modelling of the capacity fade of Li-ion cells," *J. Power Sources*, vol. 123, no. 2, pp. 230–240, 2003.

[3] Y. Zhang and C. Y. Wang, "Cycle-life characterization of automotive lithium-ion batteries with $LiNiO_2$ cathode," *J. Electrochem. Soc.*, vol. 156, no. 7, pp. A527–A535, 2009.

[4] T. Guena and P. Leblanc, "How depth of discharge affects the cycle life of lithium-metal-polymer batteries," in *Proc. IEEE Int. Telecommun. Energy Conf.*, 2006, pp. 1–8.

[5] P. Rong and M. Pedram, "An analytical model for predicting the remaining battery capacity of lithium-ion batteries," *IEEE Trans. Very Large Scale Integr. (VLSI) Syst.*, vol. 14, no. 5, pp. 441–451, May 2006.

[6] F. P. Tredeau and Z. M. Salameh, "Evaluation of lithium iron phosphate batteries for electric vehicles application," in *Proc. IEEE Veh. Power Propulsion Conf.*, 2009, pp. 1266–1270.

[7] G. Ning and B. N. Popov, "Cycle life modeling of lithium-ion batteries," *J. Electrochem. Soc.*, vol. 151, no. 10, pp. A1584–A1591, 2004.

[8] C. Rosenkranz, "Plug In hybrid batteries," in *Proc. Pres Electr. Veh. Symp. 20*, Nov. 2003, p. 14.

[9] S. B. Peterson, J. Apt, and J. F. Whitacre, "Lithium-ion battery cell degradation resulting from realistic vehicle and vehicle-to-grid utilization," *J. Power Sources*, vol. 195, no. 8, pp. 2385–2392, 2010.

[10] S. S. Choi and H. S. Lim, "Factors that affect cycle-life and possible degradation mechanisms of a Li-ion cell based on $LiCoO_2$," *J. Power Sources*, vol. 111, no. 1, pp. 130–136, 2002.

[11] B. Y. Liaw, E. P. Roth, R. G. Jungst, G. Nagasubramanian, H. L. Case, and D. H. Doughty, "Correlation of arrhenius behaviours in power and capacity fades with cell impedance and heat generation in cylindrical lithium-ion cells," *J. Power Sources*, vol. 119–121, pp. 874–886, 2003.

[12] M. Broussely, "Aging mechanisms and calendar-life predictions in lithium-ion batteries," in *Advances in Li-Ion Batteries*. New York: Springer, 2002, pp. 293–432.

[13] R. Spotnitz, "Simulation of capacity fade in lithium-ion batteries," *J. Power Sources*, vol. 113, no. 1, pp. 72–80, 2003.

[14] H. Maleki and J. N. Howard, "Effects of overdischarge on performance and thermal stability of a Li-ion cell," *J. Power Sources*, vol. 160, no. 2, pp. 1395–1402, 2006.

[15] L. Serrao, Z. Chehab, Y. Guezennee, and G. Rizzoni, "An aging model of Ni-MH batteries for hybrid electric vehicles," in *Proc. IEEE Veh. Power Propulsion Conf.*, 2005, pp. 78–85.

[16] M. Dubarry, V. Svoboda, R. Hwu, and B. Y. Liaw, "Capacity and power fading mechanisms identification from a commercial cell evaluation," *J. Power Sources*, vol. 165, no. 2, pp. 566–572, 2007.

[17] A. Millner, "Modeling lithium Ion battery degradation in electric vehicles," in *Proc. IEEE Conf. Innov. Technol. Efficient, Rel. Electr. Supply*, 2010, pp. 349–356.

[18] V. Marano, S. Onori, Y. Guezennec, G. Rizzoni, and N. Madella, "Lithium-ion batteries life estimation for plug-in hybrid electric vehicles," in *Proc. IEEE Conf. Veh. Power Propulsion Conf.*, 2009, pp. 536–543.

[19] High Power Lithium Ion APR18650M1 A123 Systems Datasheet, 2006.

[20] M. Dubarry, V. Svoboda, R. Hwu, and B. Y. Liaw, "Capacity loss in rechargeable lithium cells during cycle life testing: The importance of determining state-of-charge," *J. Power Sources*, vol. 174, no. 2, pp. 1121–1125, 2007.

[21] *Battery Test Manual for Plug-In Hybrid Electric Vehicles*. Idaho Falls: Lab. Idaho Natl., Sep. 2010.

[22] L. Lam, P. Bauer, and E. Kelder, "A practical circuit-based model for Li-ion battery cells in electric vehicle applications," in *Proc. IEEE 33rd Int. Telecommun. Energy Conf.*, 2011, pp. 1–9.

[23] S. Bhattacharya and P. Bauer, *Online State of Charge Estimation of LiFePO4 Battery for Real Electric Vehicle Driving Scenario and Modeling of the Battery Parameters for Different Driving Conditions*. Berlin, Germany: VDE Verlag, 2012.

[24] S. Bhattacharya and P. Bauer, "Requirements for charging of an electric vehicle system based on state of power (SoP) and state of energy (SoE) 2012," presented at the IEEE 7th Int. Power Electron. Motion Control Conf. ECCE Asia, Harbin, China, Jun. 2012.

[25] J. Kim, J. Shin, C. Chun, and B. Cho, "Stable configuration of a Li-Ion series battery pack based on ascreening process for improved voltage/soc balancing," *IEEE Trans. Power Electron.*, vol. 27, no. 1, pp. 411–424, Jan. 2012.

[26] L. Maharjan, T. Yamagishi, and H. Akagi, "Active-power control of individual converter cells for a battery energy storage system based on a multilevel cascade PWM converter," *IEEE Trans. Power Electron.*, vol. 27, no. 3, pp. 1099–1107, Mar. 2012.

[27] C.-H. Kim, M.-Y. Kim, H.-S. Park, and G.-W. Moon, "A modularized two-stage charge equalizer with cell selection switches for series-connected lithium-ion battery string in an HEV," *IEEE Trans. Power Electron.*, vol. 27, no. 8, pp. 3764–3774, Aug. 2012.
[28] Y. Yuanmao, K. W. E. Cheng, and Y. P. B. Yeung, "Zero-current switching switched-capacitor zero-voltage-gap automatic equalization system for series battery string," *IEEE Trans. Power Electron.*, vol. 27, no. 7, pp. 3234–3242, Jul. 2012.
[29] H. Qian, J. Zhang, J.-S. Lai, and W. Yu, "A high-efficiency grid-tie battery energy storage system," *IEEE Trans. Power Electron.*, vol. 26, no. 3, pp. 886–896, Mar. 2011.
[30] I. Aharon and A. Kuperman, "Topological overview of powertrains for battery-powered vehicles with range extenders," *IEEE Trans. Power Electron.*, vol. 26, no. 3, pp. 868–876, Mar. 2011.
[31] Z. Haihua, T. Bhattacharya, T. Duong, T. S. T. Siew, and A. M. Khambadkone, "Composite energy storage system involving battery and ultracapacitor with dynamic energymanagement in microgrid applications," *IEEE Trans. Power Electron.*, vol. 26, no. 3, pp. 923–930, Mar. 2011.
[32] J. Cao and A. Emadi, "A new battery/ultracapacitor hybrid energy storage system for electric, hybrid, and plug-in hybrid electric vehicles," *IEEE Trans. Power Electron.*, vol. 27, no. 1, pp. 122–132, Jan. 2012.
[33] F. Ongaro, S. Saggini, and P. Mattavelli, "Li-ion battery-supercapacitor hybrid storage system for a long lifetime, photovoltaic-based wireless sensor network," *IEEE Trans. Power Electron.*, vol. 27, no. 9, pp. 3944–3952, Sep. 2012.

Long Lam received the B.Sc. (*cum laude*) and M.Sc. (*cum laude*) degrees in electrical engineering from the Delft University of Technology, Delft, The Netherlands, in 2009 and 2011, respectively, and has won several thesis awards as a student. He graduated with a thesis on the state-of-health estimation of electric vehicle batteries, and was awarded the E-mobility thesis award for best thesis in the Netherlands 2011 on electric mobility.

His research interests include the areas of battery modeling, power electronics, and renewable energy integration and management. He currently works at Ecofys, Utrecht, The Netherlands, a leading consultancy in renewable energy, energy and carbon efficiency, energy systems and markets, and energy & climate policy. In Ecofys, he has worked on projects regarding market-based mechanisms for emission reduction and energy savings, competitiveness analysis, industrial roadmaps, and international industry policies. He also provides *ad hoc* knowledge support on electric vehicle batteries.

Pavol Bauer (SM'07) received the M.Sc. degree in electrical engineering from the Technical University of Kosice, Kosice, Slovakia, in 1985, and the Ph.D. degree from the Delft University of Technology, Delft, The Netherlands, in 1995.

Since 1990, he has been with the Delft University of Technology, teaching power electronics and electrical drives. From 2002 to 2003, he worked partially at KEMA, Arnhem, The Netherlands, on different projects related to power electronics applications in power systems. He received the title of Professor from the President of Czech Republic at Brno University of Technology, Brno, Czech Republic, in 2008. He has published more than 50 journal and 250 conference papers in his field, is the author or coauthor of six books, is the holder of international patents, and has organized several tutorials at international conferences. He has worked on many projects for industry concerning wind power and power electronics applications for power systems such as Smart-Trafo and participated in several Seventh Framework Programme and Leonardo da Vinci European Union projects as Project Partner and Coordinator.

Dr. Bauer is the Chairman of the IEEE Joint Industry Applications/Power Electronics/Power Engineering Society Benelux Chapter and a member of the European Power Electronics-Power Electronics and Motion Control Council and European Power Electronics Executive Committee. He is also a member of the International Steering Committee at numerous conferences.